Identification of Assistance-Dependent Neuromuscular Dynamics in Robot-Assisted Upper-Limb Rehabilitation Tasks

Amelia Gioscia[1], Stefano Mazzoleni[1,2,3], David Naso[1] and Paolo Lino[1]

***Abstract*— Robot-assisted upper-limb rehabilitation enables high-dose, task-oriented training with tunable assistance; however, the effect of assistance parameters on neuromuscular activation during functional tasks remains poorly characterized. This study investigates how Arm Weight Compensation (AWC) and grasping demand influence muscle activation during the Coffee Table task performed with the ALEx-RS exoskeleton. Six healthy subjects executed multiple AWC–grasping combinations while surface EMG was recorded from selected upper-limb muscles. Activation trends were quantified via windowed RMS profiles and subsequently modeled using linear system identification to describe the relationship between assistance levels and muscle activity. Results revealed distinct, muscle-specific modulation patterns: grasping demand predominantly drove distal muscle activation, whereas deltoid activity reflected a coupled effect of both assistance parameters. Validated dynamical models successfully captured these dependencies, providing a residual-validated characterization of assistance-dependent neuromuscular responses in healthy subjects. These findings contribute to a deeper understanding of how assistance parameters shape muscle activation during robot-assisted tasks and may inform the design of more effective, personalized rehabilitation strategies.**

I. INTRODUCTION

Stroke is a leading cause of long-term disability, and many survivors exhibit persistent upper-limb (UL) motor impairments despite standard rehabilitation [1], [2], [3]. Effective recovery requires intensive, repetitive, task specific training, but conventional therapy is limited by therapist availability and by the difficulty of objectively adapting training intensity in real time [4], [5]. Robot assisted rehabilitation enables high-dose, task oriented, and reproducible UL training with objective performance measures [6]. Exoskeletons can provide joint-aligned assistance, gravity compensation, and task-specific interaction forces [7]. The ALEx-RS (Wearable Robotics, Pisa, Italy) exoskeleton supports multi-joint UL movements through adjustable Arm Weight Compensation (AWC), grasping assistance, and integrated virtual reality exercises [8]. During functional tasks, AWC and grasping jointly modulate shoulder and forearm loading and can affect muscle activation patterns. Surface electromyography (sEMG) is widely used to quantify muscle activation, often via amplitude-based features such as the root mean square (RMS) [9], [10]. However, RMS trends alone do not explicitly capture the dynamical input–output relationship between assistance settings and target muscle activation over time. System identification provides a model-based framework to estimate dynamical mappings from measurable inputs to sEMG activation while accounting for noise and temporal dependencies [11]. Residual-based diagnostics (e.g., whiteness tests) are used to assess model adequacy. Here, we investigate how AWC and grasping levels modulate UL muscle activation during the *Coffee Table* task performed with the ALEx-RS exoskeleton in healthy subjects. We first characterize windowed RMS profiles across AWC–grasping conditions. We then apply linear system identification in two complementary analyses: (i) modeling middle deltoid activation across AWC levels, and (ii) modeling brachioradialis activation across grasping levels. For each analysis, we compare ARX, ARMAX, output-error, Box–Jenkins, and N4SID structures with residual-based validation. The contributions are: (i) a quantitative description of assistance-dependent activation trends in a functional robot-assisted task, and (ii) a residual validated comparison of linear model structures describing activation dynamics under varying AWC and grasping demand. The remainder of this paper is organized as follows. Section II presents the experimental protocol, signal-processing pipeline, feature-extraction procedure, and system-identification framework. Section III reports the obtained results in terms of RMS activation dynamics and model validation across different assistance conditions. Section IV discusses the main findings and the limitations of the proposed analysis. Finally, Section V concludes the paper and outlines future developments.

II. MATERIAL AND METHODS

A. Participants

Six right-handed healthy young adults (3 females and 3 males, age 24.17 ± 3.19 years) were enrolled in the study. None reported a history of neurological or musculoskeletal disorders, and all exhibited normal joint range of motion and muscle strength. Informed consent was obtained from all participants prior to participation. The study was conducted at the Biomedical Robotics Laboratory (BIOROB), Polytechnic University of Bari. At the beginning of each experimental session, participants were informed about the procedure.

*This work was not supported by any organization.

[1]The authors are with the Department of Electrical and Information Engineering, Politecnico di Bari, Bari, Italy a.gioscia@phd.poliba.it, stefano.mazzoleni@poliba.it, david.naso@poliba.it, paolo.lino@poliba.it

[2]The author is with IMT School for Advanced Studies Lucca, Lucca, Italy. stefano.mazzoleni@imtlucca.it

[3]The author is with the BioRobotics Institute, Scuola Superiore Sant'Anna, Pisa, Italy. stefano.mazzoleni@santannapisa.it

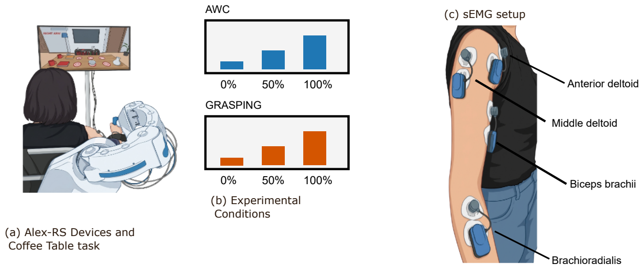

Fig. 1: Experimental setup and protocol.

B. Robotic Setup

Robotic sessions were conducted using the ALEx-RS UL exoskeleton (Arm Light Exoskeleton Rehab Station) [8], [12], [13]. The system consists of two symmetric UL exoskeleton units with adjustable spacing and can operate in bilateral or unilateral configurations. Each unit provides six degrees of freedom (DoFs): four actuated and sensorized joints (shoulder abduction/adduction, internal/external rotation, flexion/extension; elbow flexion/extension) and two sensorized only wrist DoF (wrist flexion/extension and pronation/supination). Joint positions are measured by absolute encoders, while actuation is provided by brushless motors with compliant cable transmission. The robot supports force control (end-effector forces/joint torques) and compliant position control (predefined trajectories with adjustable stiffness). At a higher level, it can run passive, assistive (impedance-based), or assisted-as-needed modalities. Across modes, gravity, friction, and inertia compensation are applied to promote smooth motion. AWC is adjusted through the graphical interface to provide gravitational offloading by generating a constant vertical support force during task execution. The system also integrates a virtual reality environment with customizable exergames and real-time exercise monitoring to enable parameter adaptation based on performance metrics.

C. EMG Recording

Surface EMG was recorded at 1000 Hz using a BTS FREEEMG-1000 wireless system (BTS Bioengineering, Milan, Italy) with pre-gelled Ag/AgCl electrodes (CE-marked; 93/42/EEC). Electrode placement followed SENIAM recommendations [14]. After skin preparation, electrodes were placed on the right upper limb over anterior deltoid (AD), middle deltoid (MD), biceps brachii (BB) (long head), and brachioradialis(BR), aligned with muscle fibers.

D. Experimental Protocol

Before each session, participants were instrumented with surface EMG electrodes and seated on the workstation chair behind the target panel frame, with the ALEx-RS exoskeleton aligned to the right acromion (robotic shoulder joint center approximately 1–3 cm from the acromial region). Subjects performed the *Coffee Table* task, a proprietary ALEx-RS virtual exercise, using the right upper limb. The task required reaching, grasping, and repositioning virtual objects according to visual cues at a self-selected comfortable speed, without robotic trajectory guidance. Task difficulty was adjusted (Table I) through two parameters: **Arm Weight Compensation (AWC)**, defines the level of robotic gravity support, and **Grasping**, defines the minimum grip force threshold required to hold virtual objects, with visual feedback provided through a grip-force bar. For each of the nine AWC–Grasping combinations, participants completed three trials in a fixed order, yielding 27 trials per participant. Trials were separated by brief intervals to ensure consistent parameter transitions. Each trial ended once all objects had been repositioned (duration $\sim$ 35–50 s). Overall, the dataset comprised 162 trials (6 subjects $\times$ 9 conditions $\times$ 3 repetitions).

TABLE I: Exercise combinations of AWC and Grasping

Combination	AWC	*Grasping*
1	0%	0%
2	0%	50%
3	0%	100%
4	50%	0%
5	50%	50%
6	50%	100%
7	100%	0%
8	100%	50%
9	100%	100%

E. Data Processing

sEMG signals were sampled at 1000 Hz (BTS FREEEMG-1000) and processed in MATLAB R2023a (Mathworks, Natick, MA, USA). For each muscle channel, subject, and trial, signals were band-pass filtered using a 2nd-order Butterworth filter (20–450 Hz) to attenuate motion artifacts and high-frequency noise. Power-line interference was reduced using a 2nd-order notch filter centered at 50 Hz (49–51 Hz stopband). All filters were applied in a zero-phase manner using forward–backward filtering to avoid phase distortion. For visualization only, the filtered signals were full-wave rectified and low-pass filtered with a 4th-order Butterworth filter ($f = 5\ Hz$) to obtain the linear envelope of muscle activation.

F. Feature Extraction

Muscle activation was quantified using the root mean square (RMS) computed from the band-pass and notch-filtered sEMG over sliding windows:

$$\mathrm{RMS}(k) = \sqrt{\frac{1}{N}\sum_{i=1}^{N} x_k(i)^2}, \tag{1}$$

where $x_k(i)$ denotes the filtered sEMG samples within the k-th window and N is the number of samples per window. RMS was computed using a 250 ms window with 50% overlap, yielding an update time $T_s = 0.125$ s for the RMS time series. This resulted in RMS time series sampled every $0.125s$ for each trial. For each condition, the three repetitions were temporally aligned and averaged to obtain a nominal RMS profile. Subject-level profiles were then aggregated to obtain group-level activation dynamics used for system identification.

G. System Identification

Preliminary analyses using the MATLAB System Identification Toolbox advisory tools did not reveal clear indications of nonlinear behavior in the considered datasets. Therefore, linear system identification models were adopted as interpretable approximations of the dominant activation dynamics within each experimental condition. Linear system identification was adopted to model input–output dynamics in the RMS activation time series during movements performed using the robotic exoskeleton. Nominal condition level profiles were first obtained by averaging the three repetitions per subject and subsequently aggregating across subjects. A single aggregated dataset was constructed and segmented by assistance level for identification. From this dataset, six level-specific subsets (AWC: 0%/50%/100%; G: 0%/50%/100%) were extracted to identify one model per level. Each subset corresponded to a specific assistance level and was modeled independently. For each target muscle, the output $y(t)$ corresponded to the RMS-based activation time series, while the input vector $u(t)$ comprised synergistic sEMG inputs and task parameters.

TABLE II: Identification tasks and model inputs

Identification task	**Output**	**sEMG inputs**	**Condition parameter**
AWC analysis	MD RMS	AD RMS, BB RMS	AWC level
Grasping analysis	BR RMS	AD RMS, BB RMS	Grasping level

The identification workflow comprised the following steps:

- **Dataset partitioning:** each level-specific RMS time series was split into estimation (70%) and validation (30%) segments, preserving temporal order (temporal hold-out).
- **Model estimation:** ARX, ARMAX, OE, BJ, and N4SID structures were estimated on the estimation segment using prediction-error minimization. Candidate model orders were explored.
- **Model validation:** performance was evaluated on the validation segment using Fit(%) together with residual diagnostics. Ljung–Box residual whiteness was treated as a necessary adequacy condition.

This procedure identified, for each level, the model structure and order that best described the nominal input–output activation dynamics.

1) ARX Model: The AutoRegressive with eXogenous input (ARX) model expresses the output as a linear combination of past outputs, past inputs, and an additive white-noise term:

$$A(q)\,y(t) = B(q)\,u(t-n_k) + e(t), \tag{2}$$

with

$$A(q) = 1 - a_1 q^{-1} - a_2 q^{-2} - \cdots - a_{n_a} q^{-n_a},$$
$$B(q) = b_1 q^{-1} + b_2 q^{-2} + \cdots + b_{n_b} q^{-n_b},$$

where q^{-1} is the unit delay operator, n_k is the input delay, and $e(t)$ is a zero-mean white-noise disturbance.

2) ARMAX: The AutoRegressive Moving Average with eXogenous input (ARMAX) model extends ARX by introducing a moving-average noise polynomial:

$$A(q)\,y(t) = B(q)\,u(t-n_k) + C(q)\,e(t), \tag{3}$$

where $A(q)$ and $B(q)$ are as above and

$$C(q) = 1 + c_1 q^{-1} + c_2 q^{-2} + \cdots + c_{n_c} q^{-n_c}.$$

3) OE: The Output-Error (OE) model represents the system dynamics through a transfer function while treating the disturbance as additive output noise:

$$y(t) = \frac{B(q)}{F(q)}\,u(t-n_k) + e(t), \tag{4}$$

where $B(q)$ and $F(q)$ parameterize the deterministic dynamics.

4) BJ: The Box–Jenkins (BJ) model separately describes system dynamics and noise dynamics:

$$y(t) = \frac{B(q)}{F(q)}\,u(t-n_k) + \frac{C(q)}{D(q)}\,e(t), \tag{5}$$

where $\frac{B(q)}{F(q)}$ models the input–output dynamics and $\frac{C(q)}{D(q)}$ captures colored disturbance dynamics.

5) N4SID: N4SID (Numerical algorithms for Subspace State Space System IDentification) estimates a discrete-time state-space model (innovation form):

$$\begin{aligned} x(t+1) &= Ax(t) + Bu(t) + Ke(t), \\ y(t) &= Cx(t) + Du(t) + e(t), \end{aligned} \tag{6}$$

where $x(t)$ denotes latent states and n_x is the chosen state dimension (selected via singular value decomposition). Subspace methods are numerically robust for multi-input systems.

H. Model Order Selection

Model parameters were estimated on the estimation segment using prediction-error minimization. For each structure (ARX, ARMAX, OE, BJ, N4SID), a set of candidate orders was explored. For polynomial models, orders $(n_a, n_b, n_c, n_d, n_f)$ and delay n_k were explored, while for N4SID the state dimension n_x was varied. Candidate configurations were evaluated on the validation segment. Residual whiteness (Ljung–Box test on validation residuals) was treated as a necessary criterion; among models satisfying the whiteness check, we selected the configuration maximizing Fit(%). The Akaike Information Criterion (AIC) was used as a parsimony indicator during order selection:

$$\begin{aligned} \text{AIC} = {} & N \log\det\left(\frac{1}{N}\sum_{t=1}^{N} \varepsilon(t,\hat{\theta}_N)\varepsilon(t,\hat{\theta}_N)^T\right) \\ & + 2n_p + Nn_y(\log(2\pi)+1), \end{aligned} \tag{7}$$

where N is the number of estimation samples, $\varepsilon(t, \hat{\theta}_N)$ is the $n_y \times 1$ prediction error vector, and n_p is the number of estimated parameters. Tables III and IV report the selected orders: ARX (n_a, n_b, n_k), ARMAX (n_a, n_b, n_c, n_k), OE (n_b, n_f, n_k), BJ $(n_b, n_c, n_d, n_f, n_k)$, N4SID (n_x).

TABLE III: Selected orders: Middle deltoid (Arm Weight Compensation)

AWC %	**Model**	**Parameters**
0	ARX	$3, 5, 0$
	ARMAX	$4, 4, 2, 0$
	OE	$5, 4, 0$
	BJ	$3, 1, 5, 4, 0$
	N4SID	7
50	ARX	$1, 4, 3$
	ARMAX	$3, 6, 7, 2$
	OE	$1, 4, 1$
	BJ	$1, 5, 1, 3, 0$
	N4SID	6
100	ARX	$5, 5, 0$
	ARMAX	$4, 1, 4, 0$
	OE	$4, 5, 1$
	BJ	$5, 1, 2, 1, 0$
	N4SID	10

TABLE IV: Selected orders: Brachioradialis (Grasping)

Grasping %	**Model**	**Parameters**
0	ARX	$5, 4, 0$
	ARMAX	$5, 3, 2, 0$
	OE	$3, 2, 0$
	BJ	$3, 2, 5, 5, 0$
	N4SID	9
50	ARX	$1, 5, 0$
	ARMAX	$5, 4, 4, 0$
	OE	$3, 5, 0$
	BJ	$2, 6, 1, 7, 0$
	N4SID	4
100	ARX	$1, 5, 0$
	ARMAX	$5, 5, 5, 0$
	OE	$4, 3, 0$
	BJ	$6, 7, 6, 8, 0$
	N4SID	10

I. Model Validation

After order selection, the identified models were evaluated on the validation dataset. Model adequacy was assessed through (i) prediction performance and (ii) residual diagnostics. Fit(%) was computed as the normalized RMS prediction error provided by the MATLAB System Identification Toolbox. Residual analysis was used to verify whether one-step-ahead prediction errors were consistent with a white process, which is a necessary condition to conclude that the model captures the dominant dynamics and that the disturbance description is appropriate. Whiteness was assessed by inspecting the residual autocorrelation function and by applying the Ljung–Box test (up to lag $m = 20$, $\alpha = 0.05$). Models failing the whiteness test were considered inadequate. Since no independent test set was available, all out-of-sample results refer to the validation segment.

III. RESULTS

This section reports (i) sEMG amplitude trends quantified via windowed RMS and (ii) the validated performance of linear model structures (ARX, ARMAX, OE, BJ, N4SID) across AWC and grasping (G) levels. Model adequacy was evaluated through prediction Fit(%) and residual diagnostics (including Ljung–Box whiteness); models failing the whiteness criterion were not considered reliable regardless of Fit. Fig. 2 shows representative windowed RMS time courses (example at $G = 100\%$) with AWC levels overlaid. A transient increase in amplitude is observed in the first 20–30 s, followed by a progressive decrease as the task progresses toward completion. MD activation increases with higher AWC particularly at higher grasping demand, whereas BR activity is primarily modulated by grasping level.

A. Modeling Middle Deltoid Across AWC

MD activation was modeled using synergistic sEMG inputs and task parameters. Table V reports Fit(%) across AWC levels for all tested model structures, with † denoting models that satisfied the Ljung–Box whiteness test on validation residuals. Although BJ and N4SID achieved higher Fit values in some conditions, they did not satisfy residual based validation consistently across AWC levels. Conversely, ARMAX provided the most consistent validated performance and was selected as the reference structure for MD modeling. Input contribution analysis indicated a dominant contribution from the BB, with AD acting as a secondary predictor. Multi-step prediction analyses showed stable long-horizon behavior with limited error growth, the results of this analysis are not reported here and will be presented in a companion paper.

TABLE V: Validation fit (%) across AWC levels. † Ljung–Box test passed.

Model	0% AWC	50% AWC	100% AWC
ARX	72.30	60.90	60.61
ARMAX	73.89†	72.15†	68.00†
OE	75.14	72.78	70.75
BJ	77.29	77.92	76.23
N4SID	69.12	80.20	52.97

B. Modeling Brachioradialis Across Grasping

BR activation was modeled using synergistic sEMG inputs and task parameters. Table VI summarizes Fit(%) across grasping levels. At $G = 0\%$ and $G = 50\%$, BJ achieved the best validated performance (Fit $\approx$ 74–75%) and passed the Ljung–Box test. At $G = 100\%$, N4SID was the only structure satisfying residual-based validation; however, prediction error increased for horizons beyond 10 steps. Overall, these findings confirm the robustness of the ARMAX structure for modeling MD activation across AWC levels, whereas BR modeling favored BJ at low-to-medium grasping (0–50%) and N4SID at high grasping (100%) when enforcing residual whiteness.

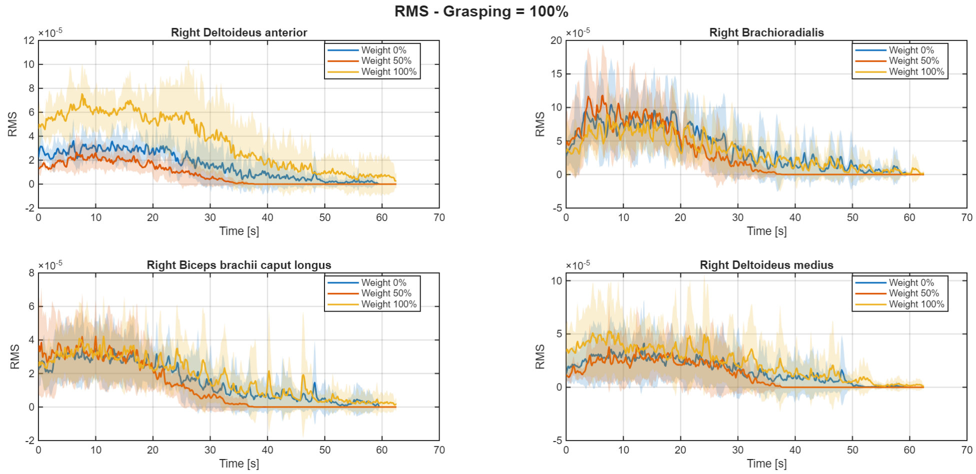

Fig. 2: Windowed RMS profiles at $G = 100\%$ across AWC levels

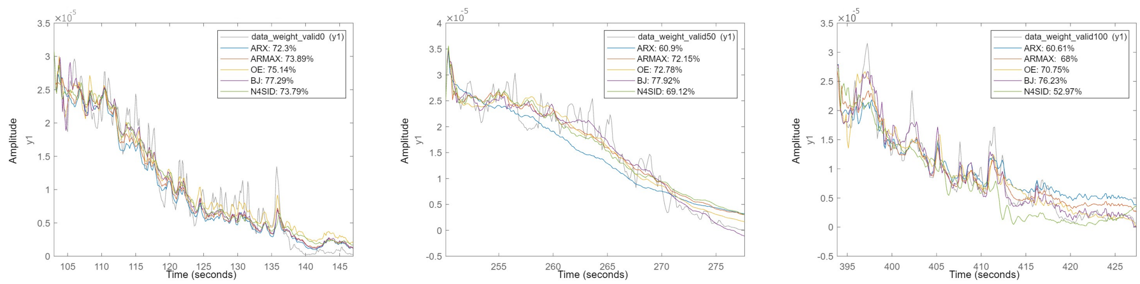

(a) (b) (c)

Fig. 3: Linear model comparison across AWC levels: (a) 0%, (b) 50%, (c) 100%.

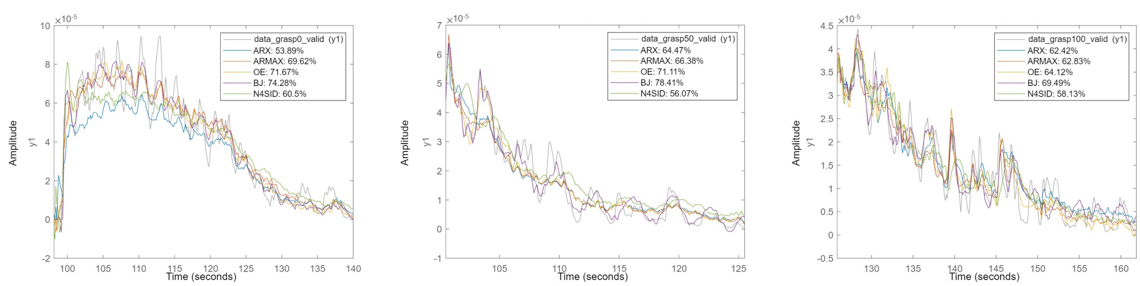

(a) (b) (c)

Fig. 4: Linear model comparison across grasping levels: (a) 0%, (b) 50%, (c) 100%.

TABLE VI: Validation fit (%) across Grasping levels. †: Ljung–Box test passed.

Model	0% G	50% G	100% G
ARX	53.89	64.74	62.42
ARMAX	69.62	66.38	62.83
OE	71.67	71.11	64.12
BJ	74.28†	74.81†	69.49
N4SID	60.50	56.07	58.13†

IV. Discussion

RMS analysis indicates that muscle activation is jointly modulated by AWC and grasping demand during the *Coffee Table* task. Proximal muscles exhibited stronger modulation under increasing assistance levels, whereas BR activity was primarily influenced by grasping demand. These trends motivated the subsequent dynamical modeling analysis. Beyond rehabilitation, this framework may also support adaptive control of occupational upper-limb exoskeletons, where assistance parameters can modulate neuromuscular load during repetitive tasks. Linear identification was used to model MD activation from synergistic sEMG inputs across AWC levels. Among the tested structures, ARMAX provided the most consistent residual-validated performance across AWC conditions. The identified input delay was $n_k = 0$ at 0% AWC, increased at 50% AWC ($n_k = 2$), and returned to $n_k = 0$ at 100% AWC, suggesting assistance-dependent changes in input–output timing. Model parameters highlighted BB as the dominant predictor across AWC levels, while the reduced AD contribution with increasing AWC likely reflects reduced shoulder elevation demand under gravity compensation, while BB contributes to task stabilization. BR activation was then modeled across grasping levels. At $G = 0\%$ and $G = 50\%$, BJ provided the best validated performance, with BB emerging as a dominant predictor. At $G = 100\%$, N4SID was the only structure satisfying residual whiteness, suggesting that a state-space representation may better capture the increased dynamical complexity associated with maximal gripping demand. However, N4SID showed reduced long-horizon prediction performance due to error accumulation in latent state estimates. The variability of the selected model orders across AWC and grasping conditions likely reflects condition-dependent changes in neuromuscular coordination and timing. Although preliminary analyses did not reveal strong nonlinear behavior, differences in optimal delays and model complexity suggest that the effective dynamics are not fully invariant across assistance levels. Therefore, the identified linear models should be interpreted as local approximations of condition-specific dynamics rather than as a single globally valid representation of the neuromuscular system. This study has some limitations. First, grasping-related dynamics were modeled using BR output only; therefore, the current formulation cannot capture the full inter-muscular coupling underlying grip regulation. Second, RMS amplitudes were not normalized to MVC; consequently, the analysis focuses on temporal dynamics and relative modulation across conditions rather than absolute activation levels. Third, identification relied on aggregated nominal profiles obtained by averaging repetitions and subjects; therefore, validation evaluates temporal hold-out prediction on aggregated signals rather than subject-specific behaviors. In addition, the limited number of healthy subjects should be considered when interpreting the generalizability of the reported findings, particularly given the known inter-subject variability of sEMG signals. The present study focused on aggregated nominal dynamics in order to characterize condition-dependent activation trends at the group level rather than subject-specific behaviors. To assess potential order-related drift due to the sequential protocol, a post hoc analysis regressing a trial-wise RMS summary (AUC over 5–35 s) against trial index found no significant group-level drift ($p = 0.162$), suggesting limited systematic fatigue or learning effects. Residual whiteness was enforced as a necessary adequacy criterion to prevent spurious model selection. Because of the limited dataset size, the same validation segment was used both for model order selection and final performance evaluation, which may introduce optimistic bias in the reported Fit values. Therefore, the reported results should primarily be interpreted as a comparative assessment of candidate model structures. Future work will extend the recording set to additional forearm and hand muscles, incorporate randomized protocols, and explore subject-level identification to support individualized model-based analysis.

V. Conclusion

This study analyzed sEMG activation during the *Coffee Table* task performed with the ALEx-RS rehabilitation robot under different AWC and grasping levels. RMS trends showed that assistance and grasping jointly modulate proximal and forearm muscle activity. Linear system identification compared ARX, ARMAX, OE, BJ, and N4SID, selecting models based on validation Fit(%) and residual whiteness. ARMAX provided the most consistent validated performance for MD across AWC levels, whereas BR modeling favored BJ at $G = 0$–50% and N4SID at $G = 100\%$. Results are based on aggregated profiles in healthy subjects and describe group-level dynamics.

References

[1] W.Johnson, O.Onuma, M.Owolabi, and S.Sachdev, "Stroke: a global response is needed", Bulletin of the World Health Organization, vol. 94, no.9, pp.634-634A, Sep. 2016.

[2] V.L.Feigin, M.Brainin, B.Norrving, et al., "World Stroke Organization: Global Stroke Fact Sheet 2025", International Journal of Stroke, vol.20, no.2, pp.132-144, 2025.

[3] S.S.Martin *et al.*, "2025 Heart Disease and Stroke Statistics: A Report of US and Global Data From the American Heart Association," Circulation, vol.151, no.8, pp.e41-e660, 2025.

[4] World Health Organization, Rehabilitation in Health Systems. Geneva, Switzerland: World Health Organization, 2017.

[5] S. F. M. Toh, K. N. K. Fong, P. C. Gonzalez, and Y. M. Tang, "Application of home-based wearable technologies in physical rehabilitation for stroke: A scoping review," IEEE Transactions on Neural Systems and Rehabilitation Engineering, vol. 31, pp. 1614–1623, 2023.

[6] J. Mehrholz, M. Pohl, T. Platz, J. Kugler, and B. Elsner, "Electromechanical and robot-assisted arm training for improving activities of daily living, arm function, and arm muscle strength after stroke," Cochrane Database of Systematic Reviews, no. 9, Art. no. CD006876, 2018.

[7] S.H.Lee, G.Park, D.Y.Cho, *et al.*, "Comparisons between end-effector and exoskeleton rehabilitation robots regarding upper extremity function among chronic stroke patients with moderate-to-severe upper limb impairment," Scientific Reports, vol.10, Art.1806, 2020.

[8] E. Pirondini, M. Coscia, S. Marcheschi, et al., "Evaluation of the effects of the arm light exoskeleton on movement execution and muscle activities: a pilot study on healthy subjects," Journal of NeuroEngineering and Rehabilitation, vol. 13, p. 9, 2016.

[9] I.Campanini, C.Disselhorst-Klug, W.Z.Rymer, and R.Merletti, "Surface EMG in Clinical Assessment and Neurorehabilitation: Barriers Limiting Its Use,"Frontiers in Neurology, vol.11, Art.934, 2020.

[10] R.Pilkar, K.Momeni, A.Ramanujam, M.Ravi, E.Garbarini, and G.F.Forrest, "Use of Surface EMG in Clinical Rehabilitation of Individuals With SCI: Barriers and Future Considerations,"Frontiers in Neurology, vol.11, Art. 78559, 2020.

[11] L.F.Sommer, C.Barreira, C.Noriega, F.Camargo-Junior, R.T.Moura, and A.Forner-Cordero, "Elbow Joint Angle Estimation with Surface Electromyography Using Autoregressive Models," in Proc. 2018 40th Annual International Conference of the IEEE Engineering in Medicine and Biology Society (EMBC), Honolulu, HI, USA, Jul. 2018, pp.1472–1475.

[12] E. Ruffaldi, M. Barsotti, D. Leonardis, G. Bassani, A. Frisoli, and M. Bergamasco, "Evaluating virtual embodiment with the alex exoskeleton," in Haptics: Neuroscience, Devices, Modeling, and Applications, M. Auvray and C. Duriez, Eds. Berlin, Heidelberg: Springer Berlin Heidelberg, 2014, pp. 133–140.

[13] F. Stroppa, S. Marcheschi, N. Mastronicola, C. Loconsole, and A. Frisoli, "Online adaptive assistance control in robot-based neurorehabilitation therapy," in 2017 International Conference on Rehabilitation Robotics (ICORR), 2017, pp. 628–633.

[14] H. J. Hermens, B. Freriks, C. Disselhorst-Klug, and G. Rau, "Development of recommendations for SEMG sensors and sensor placement procedures," *Journal of Electromyography and Kinesiology*, vol. 10, no. 5, pp. 361–374, 2000.